

DFT SIMULATIONS OF SEB RESISTANT METAL SEMICONDUCTOR INTERFACES IN SiC EPI DIODES AND MOSFETS

Jarod Worden

Virginia Polytechnic Institute and State University

Introduction

Electrical devices that have a metal/semiconductor interface, such as diodes and MOSFETs, are negatively impacted in a space radiation environment and can accumulate large defect concentrations over the course of a mission leading to the device degradation over time, or it can result in the failure when a single event effect such as Single-Event Burnout (SEB) happens due to a strike from a single high energetic ion. In order to have longer lasting and more reliable devices during a mission in a space environment, new innovation for SEB tolerant devices is necessary. Recent advances in SiC MOSFETs and diodes have demonstrated superior performance over traditional Si based devices. SiC has higher critical breakdown electric field and higher thermal conductivity leading to devices that are ideally suited to high-voltage and high-power-density power converter applications⁴. However, SiC based devices have complex interactions regarding different types of radiation damage. SiC based devices undergo SEB in high-energy ion irradiation environments that lead to a total failure in the electrical components⁵. Inclusion of SiC based devices in NASA related space programs must meet the challenges of a space radiation environment that includes energetic heavy ions, electrons, and high-energy photons, helium ions, and neutrons. Understanding the mechanisms that lead to SEB on the microscopic scale can lead to improvements in design that make SiC devices more radiation resistant.

In order to understand the SEB in different SiC based materials, Density Functional Theory (DFT) is employed to study electronic

and structural characteristics of the material. The studied interfaces include the Al-SiC interface and the h-BN-SiC interface. The h-BN-SiC interface utilizes h-BN as a 2-D material due to limiting local heating and preventing various mechanisms associated with thermal breakdown. It is important to focus on interfaces as the burnout is related to electrical instability leading to thermal load increase at the metal/semiconductor interface⁶. 4H-SiC is the primary polytype that will be examined as it has one of the highest band gap out of the four primary structures¹⁵.

Computational Methods

The calculations were conducted using first principles calculations carried out in the DFT framework using software package ABINIT¹. For self-consistent calculations, the cut-off energy was chosen to be 420 eV with an absolute change in total energy less than 10^{-5} eV. This allowed for good convergence when going through convergence testing. All cells of the atomic systems are displayed using the atomic configuration viewer Atomeye³. The Pseudopotentials used were obtained through Pseudo dojo and Harwigsen-Goedecker-Hutter pseudopotentials^{16,17}.

Results

In order to properly examine electronic structures for the 4H-SiC and the interface systems, an appropriate pseudopotential needs to be identified. Three pseudopotentials were studied based on Linear Density Approximation (LDA), Perdew-Burke-Ernzerhof (PBE), and Generalized Gradient Approximation. First, a base 4H-SiC cell is constructed as shown in

Fig. 2. The system is then relaxed using LDA exchange and correlation functional using Limited-memory Broyedn-Fletcher-Goldfarb-Shannon minimization until forces on the atoms are smaller than 5 meV/Å. Since 4h-SiC is a hexagonal lattice, the relaxed structure lattice parameters were found to be $a=b=3.056792$ Å and $c=10.008232$ Å. These values correspond well with expected values with a and c parameters within 1% of experimental results⁸. After relaxation, static calculations are done to calculate the band gap and band structure. The band structure follows the high symmetry points in the irreducible Brillouin zones. Figure 1 shows the different band structures and table 1 shows the calculated band gaps. The calculated values for band gap with these pseudopotentials display the appropriate indirect band gap but are low and do not correspond well with experimentally calculated values⁹. This issue has been documented in other DFT simulations studying the electronic properties of SiC polytypes where these potentials underrepresent band gap values^{10,11}. In order to account for this discrepancy, the hybrid potential HSE03 was used to account for this low value with correcting terms¹². Using this hybrid potential, a much better band gap value of 3.12 eV is obtained that is much closer to experimental results. Since the HSE03 reproduced band gap values the closest to the experimental value, HSE03 is the preferred potential to use.

Pseudopotential	Band gap (eV)
LDA	2.281
PBE	2.337
GGA	2.257
HSE03	3.12
Experimental	3.3

Table 1. Comparison of the band gap for different pseudopotentials

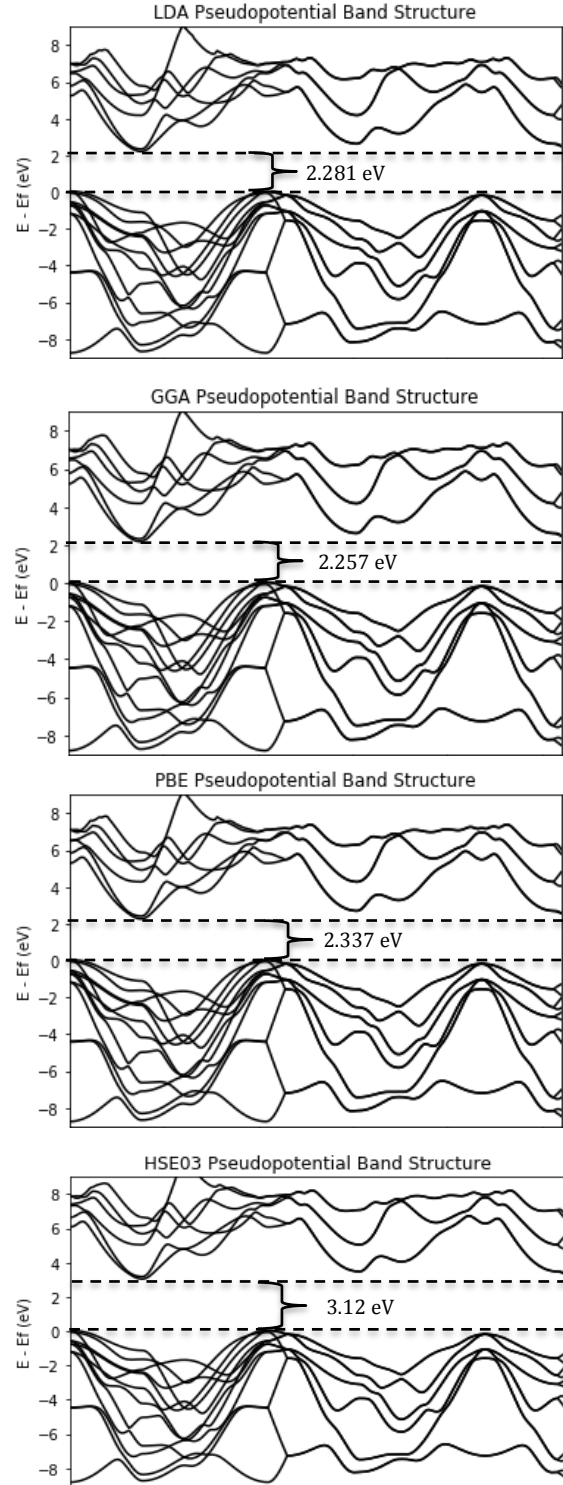


Figure 1. Band Structures for different potentials through Brillouin Zone

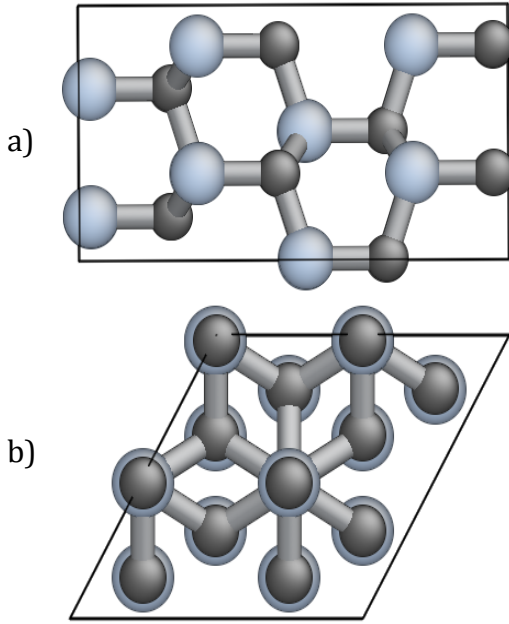


Figure 2. Base 4h-SiC cell showing a) the cell parallel to c axis and b) the cell normal to c axis. Black spheres are Carbon and Silver are Silicon.

Silicon and Carbon neutrally charged vacancy formation energies were also calculated for the bulk 4h SiC cell. Formation energy is an important value in determining the difficulty of defects to form and the concentration of defects. The calculation of defect formation energy is represented by equation 1.

$$E_f = E_V - E_0 + \mu_i \quad 1$$

In this equation, E_V is the energy of the bulk cell without defects, E_0 is the cell with the defect, and μ_i is the chemical potential of the defect, in this case the Silicon or Carbon atom. Due to the simulation cell having periodic boundary conditions, the base cell needs to be large enough such that the vacancy does not interact with itself. The cell was expanded to have 4 times the lattice parameter expanded in the a and b direction and doubled the c direction containing 256 atoms in the super cell as seen in Figure 3. A base calculation for the super cell is first done

without the vacancy and then another done with either the Carbon or Silicon removed. The results obtained displayed a value of 4.832 eV for Silicon vacancy and a value of 4.941 eV for Carbon, which are very close to other expected values¹⁸.

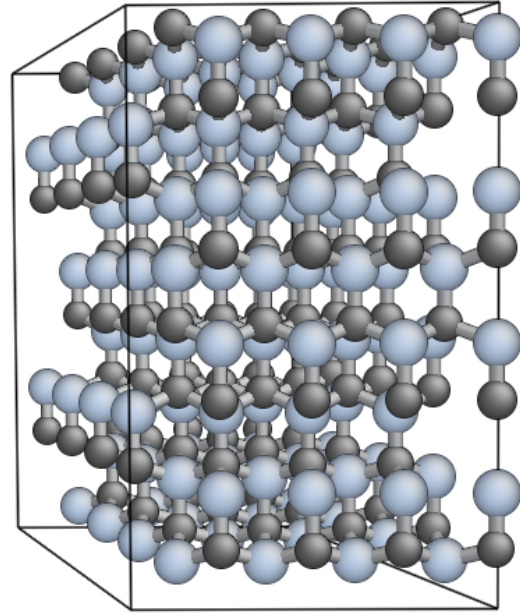


Figure 3. Super cell of 4H-SiC. Black spheres are Carbon and Silver are Silicon.

Al-SiC and Al/h-BN/SiC structures

To study the electronic response of the Al/SiC and Al/h-BN/SiC, a large super cell replicating the interfaces of the systems is produced. The method involves lining up atoms at the interface such that the atoms bond with only one other type of atomic species across the interface. Al has a face-centered cubic (fcc) structure making it difficult to maintain 1-1 bonding if the (100) surface of the Al structure tries to bind with the 4h-SiC plane perpendicular to the c axis. This can be overcome by adjusting the orientation of the Al crystal from a (100) orientation to (111). This orientation fits the

SiC hexagonal structure to allow for the 1-1 bonding. Typically, large structures are preferred when studying electronic properties to reduce charge mirroring due to the periodic boundary conditions. Thus, two super cells are constructed using 72 C, 72 Si, and 108 Al atoms with one additional cell having 9 B and 9 N atoms. The cell construction initially multiplies the a and b axes by a factor of 3 and extends the c axis to produce a SiC layer of ~ 20 Å and an Al layer of ~ 26 Å. For the Al/h-BN/SiC cell, the same dimensions are used for the SiC and Al portions, however a buffer of h-BN is placed between the Al and SiC phases. Only a singular row of h-BN is used as a 2D layer that consists of 9 B and 9 N atoms. Due to the boundary condition at the ends of the cell, vacuum layer is considered here since it prevents unphysical slab-slab interactions of charge transfer. A vacuum layer of 17 Å is considered for each initial cell. To account for possible unphysical surface-surface interaction and surface-interface interactions, hydrogen atoms are placed at the ends of the slab to passivate the surfaces to close dangling bonds and lock surface charges⁷. Once the initial cell is created, LDA potential is used to relax and obtain the final cells, which are displayed in Figure 4. The final cell dimensions for the Al/SiC system are $a=b=9.170376$ Å and $c=65.051256$ Å while the final cell dimensions for the Al-BN-SiC are $a=b=9.117094$ Å and $c=66.930172$ Å.

The increased dimension in the Al/BN/SiC in the c axis comes from the 2D layer of BN while the reduction of the a and b axes comes from the smaller primitive lattice constants of the BN. The calculated primitive hexagonal lattice constants are $a=2.82079$ Å for Al and $a=2.48898$ Å for BN. Both of these values are in good agreement with experimental results within 2%^{13,14}. In order to have the correct bond alignment for the BN-SiC interface, the BN layer was offset of the Si layer. When relaxation occurs, the BN and Si will move to have preferential binding. After relaxation, the Si was found to be most closely bonded to the N.

Interface Energy for the systems was also calculated. The equation used to calculate interface energy is given in equation 2¹⁹:

$$E_{12} = 1/A (E_1 + E_2 - E) \quad 2$$

In this equation, A is the surface area of the interface, E_1 and E_2 are the energies of the individual slabs separated by the interface, and E is the total energy of the system. The results show that the interface energy for the Al/SiC interface is -0.19345 eV/Å (which agrees well with comparative DFT calculations of -0.18288 eV/Å), and the BN/SiC interface is -0.80989 eV/Å¹⁹. The lower interface energies represent systems with higher stability as it indicates that more energy is required to break apart the bonds, showing that the inclusion of the 2D BN layer improves stability, lowering potential defect formation at the interfaces.

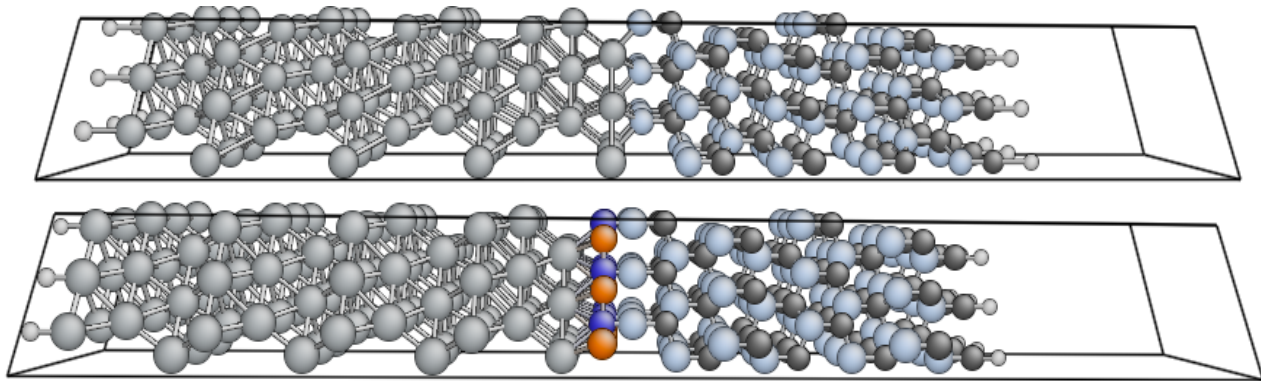


Figure 4. Super cells of the Al-SiC and Al-BN-SiC systems. Grey spheres are Al, light grey are Si, black are C, white are H, blue are N, and orange are B.

This has implications that defect formation will be reduced at the interfaces, potentially limiting long-term degradation by defect accumulation.

Conclusions

The appropriate super cells for the Al/SiC and Al/BN/SiC systems were constructed in order to study their electronic structures. 4H-SiC was first studied to analyze appropriate pseudopotentials that appropriately replicate the expected electronic values and vacancy formation energies. HSE03 exchange correlation functional was found to most closely replicate SiC systems and will be used to calculate future values for the interface systems. Interface energy calculation demonstrated higher stability when a 2D layer of h-BN is included in the system, indicating a resistance to potential defect accumulation and formation near the interface.

Future work will include more in-depth analysis in the electronic structures of the Al/SiC and Al/BN/SiC such as Fermi surfaces to determine electron and hole pockets, band structures, hopping integral, barrier height, and other properties. To study the thermal properties, such as phonon dispersion and group velocities, finite strain method will be used to calculate elastic constants coupled to continuum elastic wave equations. The transient and steady state coupled behavior of electron and phonon transport through bulk and across interface will be examined in the framework of Steepest Entropy Ascent Quantum Thermodynamics through inputs of density of states and phonon dispersion. This will provide analysis on heat release and temperature evolutions at the interface, electrical conductivity, transition temperature, critical current density, threshold SEB, and other properties.

References

- [1] Gonze, X. *et al.* The Abinitproject: Impact, environment and recent developments. *Computer Physics Communications* **248**, 107042 (2020).
- [2] Nocedal, J. Updating Quasi-Newton Matrices With Limited Storage. (1980) doi:10.1090/S0025-5718-1980-0572855-7.
- [3] J. Li, AtomEye: an efficient atomistic configuration viewer, *Modeling Simulation in Material Science Engineering*, 11 (2003) 173-177
- [4] A.F. Witulski, D.R. Ball, A.L. Sternberg, K.F. Galloway, A.Javanainen, J-M. Lauenstein, R.D. Schrimpf. Single-Event Burnout Mechanisms in SiC Power MOSFETs. *IEEE Trans. Nucl. Sci.*, **65** (8), 1951 (2018).
- [5] A.F. Witulski, D.R. Ball, R.A. Johnson, et. al. New Insight into Single-Event Radiation Failure Mechanisms in Silicon Carbide Power Schottky Diodes and MOSFETs. *Materials Science Forum*, **1004**, pp.1066-1073 (2020).
- [6] C. Abbate, G. Busatto, P. Cova, N. Delmonte, F. Giuliani, F. Iannuzzo, A. Sanseverino, F. Velardi. Analysis of Heavy Ion Irradiation Induced Thermal Damage in SiC Schottky Diodes. *IEEE Transactions on Nuclear Science*, **62** (1), 202 (2015).
- [7] Wang, X. *et al.* Density functional theory calculation of the properties of carbon vacancy defects in silicon carbide. *Nanotechnology and Precision Engineering* **3**, 211–217 (2020)
- [8] Stockmeier, M., Müller, R., Sakwe, S. A., Wellmann, P. J. & Magerl, A. On the lattice parameters of silicon carbide. *Journal of Applied Physics* **105**, 033511 (2009).
- [9] Lüning, J., Eisebitt, S., Rubensson, J.-E., Ellmers, C. & Eberhardt, W. Electronic structure of silicon carbide polytypes studied by soft x-ray spectroscopy. *Phys. Rev. B* **59**, 10573–10582 (1999).
- [10] Sinelnik, A. V. & Semenov, A. V. Theoretical study of the band structure of 2H-SiC and 4H-

- SiC of silicon carbide polytypes. *Condens. Matter Phys.* **24**, 23705 (2021).
- [11] Perdew, J. P. *et al.* Understanding band gaps of solids in generalized Kohn–Sham theory. *Proceedings of the National Academy of Sciences* **114**, 2801–2806 (2017).
- [12] Lacks, D. J. & Gordon, R. G. Pair interactions of rare-gas atoms as a test of exchange-energy-density functionals in regions of large density gradients. *Phys. Rev. A* **47**, 4681–4690 (1993).
- [13] Tang, F. L. *et al.* Surface structure and solidification morphology of aluminum nanoclusters. *Physica B: Condensed Matter* **404**, 2489–2494 (2009).
- [14] Xu, B. *et al.* Lattice Parameters of Hexagonal and Cubic Boron Nitrides at High Temperature and High Pressure. *Integrated Ferroelectrics* **162**, 85–93 (2015).
- [15] Persson, C., Lindefelt, U. & Sernelius, B. E. Band gap narrowing in *n*-type and *p*-type 3C-, 2H-, 4H-, 6H-SiC, and Si. *Journal of Applied Physics* **86**, 4419–4427 (1999).
- [16] van Setten, M. J. *et al.* The PseudoDojo: Training and grading a 85 element optimized norm-conserving pseudopotential table. *Computer Physics Communications* **226**, 39–54 (2018).
- [17] Krack, M. Pseudopotentials for H to Kr optimized for gradient-corrected exchange-correlation functionals. *Theor Chem Acc* **114**, 145–152 (2005).
- [18] Wang, X. *et al.* Density functional theory calculation of the properties of carbon vacancy defects in silicon carbide. *Nanotechnology and Precision Engineering* **3**, 211–217 (2020).
- [19] Wang, C., Chen, W., Jia, Y. & Xie, J. Calculating Study on Properties of Al (111)/6H-SiC (0001) Interfaces. *Metals* **10**, 1197 (2020).